



A Journal of the Gesellschaft Deutscher Chemiker

# Angewandte Chemie

GDCh

International Edition

www.angewandte.org

## Accepted Article

**Title:** Tuning Cu/Cu<sub>2</sub>O Interfaces for Reduction of Carbon Dioxide to Methanol in Aqueous Solutions

**Authors:** Jinlong Gong, Xiaoxia Chang, Tuo Wang, Zhijian Zhao, Piaoping Yang, Jeffrey Greeley, Rentao Mu, Gong Zhang, Zhongmiao Gong, Zhibin Luo, Jun Chen, Yi Cui, and Geoffrey Ozin

This manuscript has been accepted after peer review and appears as an Accepted Article online prior to editing, proofing, and formal publication of the final Version of Record (VoR). This work is currently citable by using the Digital Object Identifier (DOI) given below. The VoR will be published online in Early View as soon as possible and may be different to this Accepted Article as a result of editing. Readers should obtain the VoR from the journal website shown below when it is published to ensure accuracy of information. The authors are responsible for the content of this Accepted Article.

**To be cited as:** *Angew. Chem. Int. Ed.* 10.1002/anie.201805256  
*Angew. Chem.* 10.1002/ange.201805256

**Link to VoR:** <http://dx.doi.org/10.1002/anie.201805256>  
<http://dx.doi.org/10.1002/ange.201805256>

# Tuning Cu/Cu<sub>2</sub>O Interfaces for Reduction of Carbon Dioxide to Methanol in Aqueous Solutions

Xiaoxia Chang<sup>†</sup>, Tuo Wang<sup>†</sup>, Zhi-Jian Zhao, Piaoping Yang, Jeffrey Greeley, Rentao Mu, Gong Zhang, Zhongmiao Gong, Zhibin Luo, Jun Chen, Yi Cui, Geoffrey A. Ozin, and Jinlong Gong<sup>\*</sup>

**Abstract:** Artificial photosynthesis can store solar energy and reduce CO<sub>2</sub> into fuels to potentially alleviate global warming and energy crisis. Compared to gas products, it remains a grand challenge to tune the product distribution of artificial photosynthesis to liquid fuels, such as CH<sub>3</sub>OH, that are suitable for storage and transport. This paper describes the introduction of metallic Cu nanoparticles (NPs) on Cu<sub>2</sub>O films to change the product distribution from gas products on bare Cu<sub>2</sub>O to predominant CH<sub>3</sub>OH via CO<sub>2</sub> reduction in aqueous solutions. The specifically designed Cu/Cu<sub>2</sub>O interfaces could balance the binding strengths of H<sup>+</sup> and CO<sup>•</sup> intermediates, which plays critical roles in CH<sub>3</sub>OH production. With TiO<sub>2</sub> model photoanode to construct a photoelectrochemical cell, Cu/Cu<sub>2</sub>O dark cathode exhibited a Faradaic efficiency up to 53.6% for CH<sub>3</sub>OH production. This work demonstrates the feasibility and mechanism of interface engineering to enhance the CH<sub>3</sub>OH production from CO<sub>2</sub> reduction in aqueous electrolytes.

Solar power is a clean, renewable and abundant energy source, which can be utilized to reduce CO<sub>2</sub> into fuels and chemicals.<sup>[1]</sup> However, the reduction of CO<sub>2</sub> with H<sub>2</sub>O is confronted with fierce competition from the H<sub>2</sub> evolution reaction (HER), together with a wide product distribution due to many possible reaction pathways.<sup>[2]</sup> Liquid products of CO<sub>2</sub> reduction, such as CH<sub>3</sub>OH, are more suitable for storage and transport as fuels or chemical feedstocks. The utilization of CH<sub>3</sub>OH could become very important in the development of a sustainable society.<sup>[3]</sup> Unfortunately, the involved six-proton-coupled six-electron-transfer processes make it much more difficult to produce CH<sub>3</sub>OH than the two-electron-reduced products of CO/HCOOH. Although Bocarsly and co-workers have achieved

CH<sub>3</sub>OH production with nearly unity FE via CO<sub>2</sub> reduction in pyridine,<sup>[3a]</sup> selectively targeting CH<sub>3</sub>OH at a high yield in aqueous solutions is still a grand challenge. Rajeshwar and co-workers have reported CH<sub>3</sub>OH production at a FE of ~95% over CuO-Cu<sub>2</sub>O arrays in aqueous solution, which is speculated from the current-potential curves.<sup>[4]</sup> Wei et al. have performed the CH<sub>3</sub>OH generation with a FE of 88% over CdSeTe/TiO<sub>2</sub> electrode, which however omits the detection of gas products.<sup>[5]</sup>

Many recent studies on CO<sub>2</sub> reduction and related reactions have primarily focused on designing copper-based materials owing to their low toxicity, high abundance, unique catalytic activity and good stability. Systematic investigations have been performed to reveal the active sites and Cu-oxide interfacial interaction over Cu-based industrial and electrochemical CO<sub>2</sub> hydrogenation catalysts.<sup>[6]</sup> In our previous work, a CO<sub>2</sub> reduction system containing Cu<sub>2</sub>O dark cathode was demonstrated to continuously suppress HER and enhance the generation of gaseous CO and CH<sub>4</sub> products in CO<sub>2</sub> reduction for up to 6 h reaction.<sup>[7]</sup> However, the generation of CH<sub>3</sub>OH was limited since this process requires an appropriate binding strength of CO<sup>•</sup> intermediate and sufficient surface adsorbed hydrogen (H<sup>+</sup>) rather than protons in the solution for the further reduction and hydrogenation of CO<sup>•</sup>.<sup>[8]</sup> Although Cu(I) species were proposed to be the active sites for selective CH<sub>3</sub>OH generation by some previous studies on Cu<sub>2</sub>O NPs,<sup>[9]</sup> there is no catalytic system developed yet to successfully manipulate the binding strengths of H<sup>+</sup> and CO<sup>•</sup> as the descriptors to optimize CH<sub>3</sub>OH production in CO<sub>2</sub> reduction. Therefore, Cu<sub>2</sub>O is taken as a model cathode, on which the binding strengths of H<sup>+</sup> and CO<sup>•</sup> are too weak and too strong, respectively (see DFT and experimental results shown below), to optimize these two descriptors for the selective production of CH<sub>3</sub>OH. In this study, metallic Cu NPs were introduced onto Cu<sub>2</sub>O films to obtain an explicitly defined structure of Cu/Cu<sub>2</sub>O interface for enhanced H<sup>+</sup> binding and reduced CO<sup>•</sup> binding, resulting in an increased FE up to 53.6% for CH<sub>3</sub>OH generation via aqueous CO<sub>2</sub> reduction in conjunction with a TiO<sub>2</sub> photoanode in photoelectrochemical (PEC) cell, which is among the highest FE ever reported in aqueous solutions over non-noble catalysts.<sup>[9]</sup> Through thermodynamic and kinetic analysis on CH<sub>3</sub>OH production over Cu/Cu<sub>2</sub>O films with different Cu amounts, Cu/Cu<sub>2</sub>O interface is demonstrated to be the dominant factor in CH<sub>3</sub>OH production since the interfacial sites play critical roles in catalysis.<sup>[6c, 10]</sup>

In order to investigate the properties of Cu/Cu<sub>2</sub>O interface individually, Cu<sub>2</sub>O model cathode with a film thickness of ~1 μm is electrodeposited on Cu substrate and exhibits a smooth surface with a predominant (111) orientation (Figure S1 and S2a).<sup>[11]</sup> X-ray photoelectron spectroscopy (XPS) of Cu<sub>2</sub>O film reveals the absence of Cu<sup>2+</sup> peaks, indicating that the obtained

[\*] Dr. X. Chang, Dr. T. Wang, Dr. Z. Zhao, P. Yang, Dr. R. Mu, G. Zhang, Z. Luo, Prof. Dr. J. Gong  
Key Laboratory for Green Chemical Technology of Ministry of Education, School of Chemical Engineering and Technology, Tianjin University; Collaborative Innovation Center of Chemical Science and Engineering, Tianjin 300072, China  
E-mail: [jlgong@tju.edu.cn](mailto:jlgong@tju.edu.cn)  
Prof. Dr. J. Greeley  
Davidson School of Chemical Engineering, Purdue University, West Lafayette, Indiana 47907, United States  
Z. Gong, Dr. Y. Cui  
Vacuum Interconnected Nanotech Workstation, Suzhou Institute of Nano-Tech and Nano-Bionics, Chinese Academy of Sciences, Suzhou 215123, China  
Dr. J. Chen  
Department of Materials Science and Engineering, Stanford University, Stanford, California 94305, United States  
Prof. Dr. G. Ozin  
Department of Chemistry, University of Toronto, Toronto, Canada  
Dr. X. Chang, and Dr. T. Wang contributed equally to the creation of this work.  
Supporting information for this article is given via a link at the end of the document.

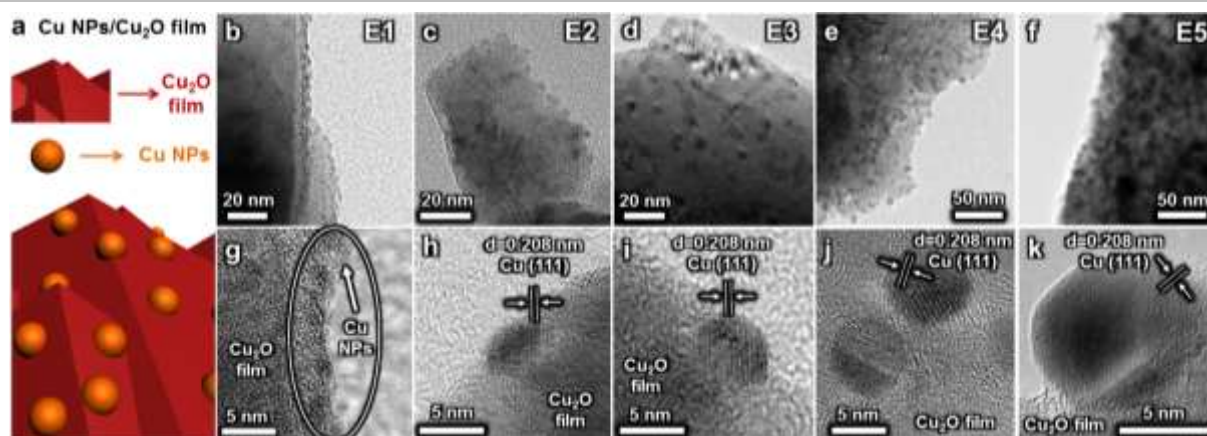


**Figure 1.** (a) Schematic, (b-f) TEM images and (g-k) HRTEM images of Cu NPs/Cu<sub>2</sub>O film. The particle sizes of Cu NPs were determined via averaging at least 50 particles.

electrodes were not oxidized in air (Figure S2b). Cu NPs were loaded onto Cu<sub>2</sub>O film using e-beam evaporation, employing a quartz crystal microbalance (QCM) to monitor the loading amount. Five samples denoted as E1-E5 with different Cu loading amounts were selected to investigate the interfacial effects. The nucleation of Cu on Cu<sub>2</sub>O surface followed an island growth mechanism,<sup>[12]</sup> resulting in the formation of Cu NPs with a predominant (111) orientation (Figure 1). The average particle diameters of Cu are  $1.5 \pm 0.1$ ,  $3.4 \pm 0.2$ ,  $5.4 \pm 0.4$ ,  $7.1 \pm 0.5$  and  $8.6 \pm 0.5$  nm for E1-E5, respectively, as evidenced by transmission electron microscopy (TEM) and high-resolution TEM (HRTEM) images in Figure 1 (size distribution in Figure S3). TiO<sub>2</sub> nanorod (NR) model photoanode was obtained by a facile hydrothermal method to construct a PEC cell with Cu/Cu<sub>2</sub>O cathode for CO<sub>2</sub> reduction. In addition, bare metallic Cu NPs were deposited on inert glassy carbon electrode (GCE) with the same loading amount as E2 for comparison.

The CO<sub>2</sub> reduction reactions were conducted in CO<sub>2</sub>-saturated 0.1 M KHCO<sub>3</sub> (pH 6.9) in a Nafion-separated two-compartment cell using a typical three-electrode configuration with TiO<sub>2</sub> NRs as the working electrode (WE) under illumination and external bias, saturated Ag/AgCl as reference electrode (RE), and Cu NPs, Cu<sub>2</sub>O film and Cu/Cu<sub>2</sub>O films as counter electrodes (CE) in darkness (dark cathodes), respectively (Figure S4). TiO<sub>2</sub> photoanode with a high photovoltage under air mass 1.5 global (AM 1.5G) plays a critical role in improving the stability of Cu<sub>2</sub>O, attributing to the highly energetic electrons and large potential exerted on cathode for preferential CO<sub>2</sub> reduction as well as the moderate current density that inhibits corrosion, which could not be achieved through electrocatalysis over Cu<sub>2</sub>O (Figure S5 and S6).<sup>[7, 13]</sup> Thus, TiO<sub>2</sub> is a suitable photoanode to maintain the stability of Cu<sub>2</sub>O cathodes and to investigate their surface catalytic properties. To facilitate the comparison with previous studies, all the CO<sub>2</sub> reduction reactions were conducted by applying 100 mW cm<sup>-2</sup> AM 1.5G and a constant external bias of 0.75 V vs. the reversible hydrogen electrode (RHE) on TiO<sub>2</sub> WE. The potential on Cu<sub>2</sub>O dark cathode and the average current density in the circuit were measured to be about -0.7 V vs. RHE and 1.3 mA cm<sup>-2</sup>, respectively, during the reaction under these conditions (Figure S6a). In contrast to the Cu/GCE and Cu<sub>2</sub>O film dark cathodes with gaseous H<sub>2</sub>/CO/CH<sub>4</sub> as main products (Figure 2a and b), Cu/Cu<sub>2</sub>O films exhibit a great enhancement for CH<sub>3</sub>OH generation (Figure 2c, d and S7),

which is ascribed to the interface between Cu NPs and Cu<sub>2</sub>O film. With increasing Cu NPs loading amount and particle size, CH<sub>3</sub>OH evolution shows a volcano-like trend and E2 exhibits the maximum CH<sub>3</sub>OH production with a FE of 53.6%, which is among the highest for CO<sub>2</sub> reduction in aqueous solutions (Figure 2e, Table S1 and S2). It is worthy to note that the size range of deposited Cu NPs in this work (1.5–8.6 nm) could rule out the size effect on product selectivity according to previous studies on CO<sub>2</sub> reduction over Cu NPs with different sizes.<sup>[14]</sup>

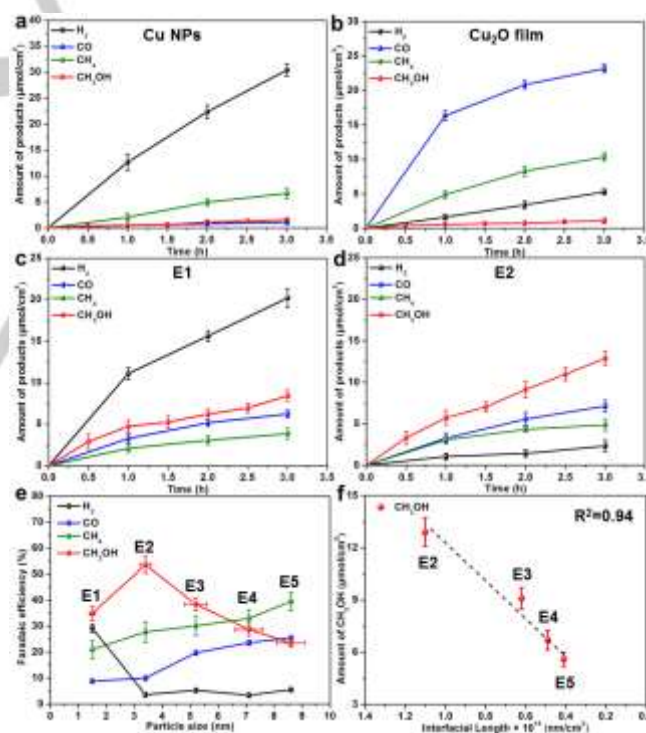


**Figure 2.** (a, b, c and d) The product amounts normalized to the geometric area of GCE or Cu<sub>2</sub>O electrodes as a function of reaction time using TiO<sub>2</sub> NRs as WE, saturated Ag/AgCl as RE, bare Cu NPs, Cu<sub>2</sub>O film, E1 and E2 as CE, respectively. (e) The dependence of FE on the Cu NP size. (f) The dependence of CH<sub>3</sub>OH generation amount on the Cu/Cu<sub>2</sub>O interfacial length.

To quantify the interface between Cu NPs and Cu<sub>2</sub>O film, the Cu NPs were treated as spheres with half inserted into Cu<sub>2</sub>O

surface, which is a reasonable simplification according to TEM and HRTEM images (Figure 1). Therefore, the Cu NP numbers and Cu/Cu<sub>2</sub>O interfacial lengths could be estimated based on loading mass and particle size (Table S3), which decrease gradually with increasing Cu particle size (from E1 to E5). With a minor Cu loading amount on E1, the Cu NPs are featured by very small sizes with a high density, thus nearly covering all the Cu<sub>2</sub>O surface (as estimated in Table S3 and Figure S8), which is consistent with the growth mechanism of glancing angle deposition<sup>[12]</sup> and leads to insufficient exposure of Cu<sub>2</sub>O and Cu/Cu<sub>2</sub>O interface. Thus, CO<sub>2</sub> reduction occurred predominantly on the surface of metallic Cu, resulting in a similar performance to the Cu/GCE electrode and yielding a large amount of H<sub>2</sub>. With increasing Cu loading amount (E2-E5), the adjacent small Cu NPs would aggregate to form larger ones and the Cu/Cu<sub>2</sub>O interface could be exposed.<sup>[15]</sup> It can be seen that the CH<sub>3</sub>OH evolution amounts show an approximate linear relationship with the lengths of Cu/Cu<sub>2</sub>O interface (Figure 2f), strongly suggesting that most CH<sub>3</sub>OH come from the interfacial sites. In addition, the TEM and SEM images of E2 after the reaction indicate the good maintenance of surface structure (Figure S9).

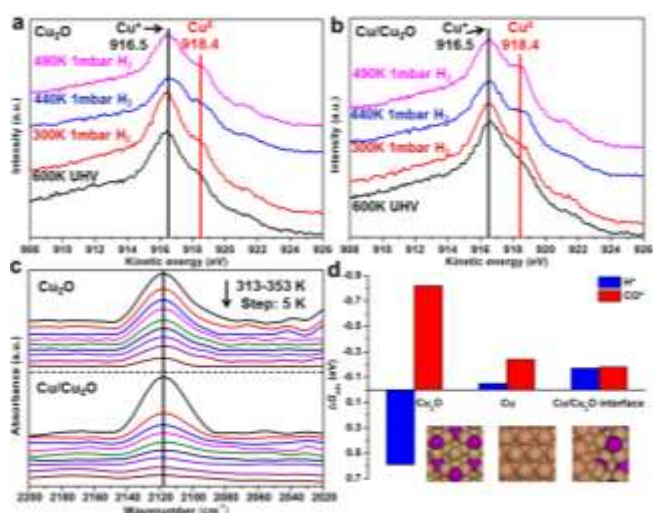


**Figure 3.** (a, b) The Cu LMM Auger spectra for Cu<sub>2</sub>O and Cu/Cu<sub>2</sub>O under various conditions. (c) FTIR spectra of CO\* adsorbed on Cu<sub>2</sub>O and Cu/Cu<sub>2</sub>O. (d) The calculated free energies of H\* and CO\* after entropy correction on different sites. Insets are models of Cu<sub>2</sub>O(111), Cu(111) and the interface.

Furthermore, ambient pressure XPS (APXPS), Fourier transform infrared spectroscopy (FTIR) in the reflection mode, and DFT calculations were applied to investigate the H\* and CO\* adsorption properties, which play critical roles in CH<sub>3</sub>OH production, on Cu, Cu<sub>2</sub>O and Cu/Cu<sub>2</sub>O interface (Figure 3). Prior to the measurements of APXPS, the samples were annealed at 600 K in ultrahigh vacuum (UHV) to remove surface impurities. With increasing annealing temperature, the peak of hydroxyl, formed by adsorbing H\* on O atoms in Cu<sub>2</sub>O,<sup>[16]</sup> at 531.4 eV decreases gradually. The Cu/Cu<sub>2</sub>O sample exhibits a much slower decrease of hydroxyl signal, indicating its stronger H\* binding strength compared to the Cu<sub>2</sub>O sample (Figure S10a). After cooling down in UHV, H<sub>2</sub> was introduced and surface

adsorbed H\* was formed to reduce Cu<sup>+</sup> into Cu<sup>0</sup>. Compared to bare Cu<sub>2</sub>O (Figure 3a), Cu/Cu<sub>2</sub>O (Figure 3b) exhibits a much more prominent generation rate of Cu<sup>0</sup> peak (918.4 eV)<sup>[17]</sup> at 1 mbar H<sub>2</sub> as the temperature rises from 300 K to 490 K, which is visualized by the larger slope for the increase of Cu<sup>0</sup>/Cu<sup>+</sup> peak area ratio (Figure S11a).

In addition, H<sub>2</sub> temperature-programmed desorption (TPD) results also indicate stronger H\* binding on Cu/Cu<sub>2</sub>O (Figure S10b). Furthermore, with increasing temperature from 313 K to 353 K, the peak of adsorbed CO\* on Cu<sub>2</sub>O (2117.8 cm<sup>-1</sup>)<sup>[18]</sup> in FTIR decreases much more slowly than that on Cu/Cu<sub>2</sub>O, indicating the much stronger CO\* binding on Cu<sub>2</sub>O<sup>[19]</sup> and the reduced CO\* binding strength on Cu/Cu<sub>2</sub>O (Figure 3c and S11b). DFT calculations (Figure 3d) provide further evidence of the extremely weak and strong adsorption of H\* and CO\*, respectively, on Cu<sub>2</sub>O. In contrast, Cu/Cu<sub>2</sub>O interface exhibits enhanced H\* adsorption and reduced CO\* adsorption, both of which are favorable to CH<sub>3</sub>OH production. At microscopic level, a simple qualitative explanation for the stronger H\* adsorption and weaker CO\* adsorption is that the Cu/Cu<sub>2</sub>O interface offers appropriate adsorption sites. Specifically, H\* can not only bind to Cu<sub>2</sub>O but also bind to metallic Cu, leading to a more stable adsorption. On the other hand, CO\* binding is much stronger on Cu<sub>2</sub>O due to the coordinatively unsaturated Cu atoms. However, according to the Bader charge analysis (Table S4), the positive charge of coordinatively unsaturated Cu at the Cu/Cu<sub>2</sub>O interface becomes less positive by 0.12 e compared to that on Cu<sub>2</sub>O, leading to a weaker CO\* adsorption at the interfacial site.

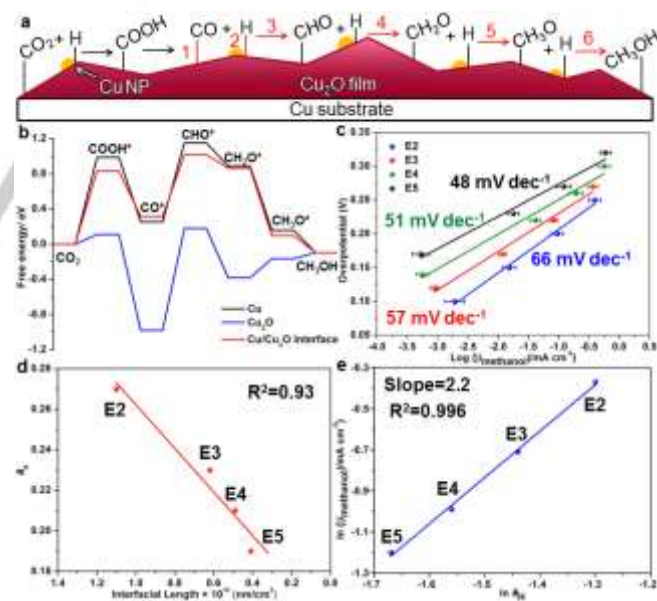


**Figure 4.** (a) The schematic reaction mechanism of CO<sub>2</sub>\* reduction to CH<sub>3</sub>OH\* on the surface of Cu/Cu<sub>2</sub>O. (b) Energy profile from DFT calculations for CO<sub>2</sub> reduction to CH<sub>3</sub>OH on different sites at 0 V vs. RHE. (c) Tafel curves of CH<sub>3</sub>OH production for samples E2-E5 measured by using them as WE, Pt as CE and saturated Ag/AgCl as RE. (d) The relationship between  $\theta_H$  and Cu/Cu<sub>2</sub>O interfacial length. (e) The logarithm of CH<sub>3</sub>OH partial current as a function of  $\ln \theta_H$ .

The reaction mechanism was investigated through thermodynamic and kinetic studies based on DFT calculations and Tafel analysis. The Cu(111) and Cu<sub>2</sub>O(111) were chosen as the model surfaces for DFT calculations according to the measured lattice spacing values in HRTEM images (Figure 1 and S1) and the fact that Cu<sub>2</sub>O(111) is the most thermodynamically stable facet of Cu<sub>2</sub>O with the lowest surface energy.<sup>[20]</sup> Furthermore, the lowest free energy pathway for CO<sub>2</sub> reduction to CH<sub>3</sub>OH at 0 V vs. RHE can be concluded based on our calculated adsorption energies of various intermediates on the three reaction sites (Figure 4a, b and S12; Table S5 and S6). The formation of key intermediate CHO\* (step 3 in Figure 4a) is a potential-limiting step in thermodynamics for CH<sub>3</sub>OH generation over all the reaction sites due to its largest uphill change in free energy ( $\Delta G > 0$ ).<sup>[8d, 21]</sup> Cu/Cu<sub>2</sub>O interface exhibits the lowest  $\Delta G$  for step 3, suggesting that the interface is more beneficial for CHO\* formation.

In addition to thermodynamics, kinetic studies were also conducted based on Tafel analysis (details in Supplemental Information). The samples E2-E5 possess Tafel slopes of 66, 57, 51 and 48 mV dec<sup>-1</sup>, respectively, for CH<sub>3</sub>OH production (Figure 4c), which are very close to 59 mV dec<sup>-1</sup> and suggest a reduction mechanism involving a fast initial single electron reduction of CO<sub>2</sub> and a subsequent slower hydrogenation process as the rate-determining step.<sup>[22]</sup> It has been widely accepted that CO\* is the key intermediate in CO<sub>2</sub> reduction and the precursor for hydrocarbon generation on copper based catalysts, which indicates that the product distribution is determined by the subsequent hydrogenation process of CO\*. Therefore, in order to conveniently investigate the rate-limiting step for CH<sub>3</sub>OH generation, it is proposed that CO\* molecules initially adsorbed on the surface of catalysts, followed by subsequent reduction steps into CH<sub>3</sub>OH (marked with red in Figure 4a). Since the first hydrogenation of CO\* (step 3 in Figure 4a) has an uphill  $\Delta G$  and may be the rate-limiting step (Figure 4b), the CH<sub>3</sub>OH partial current can be described as follows with the other reactions in equilibrium.

$$i = n F k_3 \theta_{CO} \theta_H = \frac{n F k_3 K_2 P_{CO} \theta_H^2}{K_1 [H^+] \exp\left(\frac{-EF}{RT}\right)} \quad (1)$$

where  $i$  is the partial current of CH<sub>3</sub>OH,  $\theta_H$  is the surface coverage of H\* and  $E$  is the applied potential. Meanwhile, combining Nernst equation and the definition of Tafel slope, the expression of Tafel slope can be described as equation 2.

$$\text{Tafel slope} = -\frac{\partial \ln i}{\partial E} = \frac{2.3 RT}{2 F (1 - 2\theta_H)} \quad (2)$$

Therefore, the surface coverages of H\* for E2-E5 are estimated to be 0.27, 0.23, 0.21 and 0.19, respectively, according to the experimental results of Tafel slopes in Figure 4c (results summarized in Table S7). It can be seen that  $\theta_H$  shows an approximate linear relationship with Cu/Cu<sub>2</sub>O interfacial length (Figure 4d) but no specific relationship with the total surface area of Cu NPs (Figure S13), indicating that almost all

the H\* species for CH<sub>3</sub>OH generation are adsorbed on interfacial sites. In addition, equation 1 can also be described as:

$$\ln i = 2 \ln \theta_H + \ln \frac{n F k_3 K_2 P_{CO}}{K_1} - \ln [H^+] + \frac{EF}{RT} \quad (3)$$

which indicates the theoretical two-order dependence between  $\ln i$  and  $\ln \theta_H$ . On the other hand, the relationship between  $\ln i$  and  $\ln \theta_H$  can be established through the experimental results of CO<sub>2</sub> reduction in PEC cell (Figure 2 and S7; Table S1) and Tafel slope measurements (Figure 4c). The linear fitted line obtained from experimental results shows a slope of 2.2 (Figure 4e), which is very close to the theoretical value of 2 in equation 3. Therefore, both the theoretical analysis and experimental results confirm that the first hydrogenation of CO\* is indeed the rate-limiting step for all the samples and Cu/Cu<sub>2</sub>O interface plays a critical role in the binding of H\* and the production of CH<sub>3</sub>OH.

In summary, a common challenge exists in CO<sub>2</sub> reduction in aqueous solutions, namely the competition between proton reduction and surface adsorbed H\* reduction, where the latter largely determines the CH<sub>3</sub>OH generation. Meanwhile, the binding strength of CO\* intermediates needs to be controlled to an appropriate level to facilitate the subsequent hydrogenation process. In this work, an electrode with structurally tunable Cu/Cu<sub>2</sub>O interface is constructed for the enhanced H\* binding and reduced CO\* binding compared to the original Cu<sub>2</sub>O surface, which effectively tunes the product distribution and increases the production of CH<sub>3</sub>OH to a high FE of 53.6%. This work will provide new insights into controlling the product distribution of CO<sub>2</sub> reduction and develop a new method for high-efficiency, low-cost and stable CH<sub>3</sub>OH generation. If Cu NPs could be selectively deposited onto the edge sites of Cu<sub>2</sub>O film, more reactive Cu/Cu<sub>2</sub>O interfacial sites might be generated to further boost the production of CH<sub>3</sub>OH, which calls for more future investigations.

## Acknowledgements

We acknowledge the National Key R&D Program of China (2016YFB0600901), the National Natural Science Foundation of China (21525626, U1463205, U1662111, 21722608, 51861125104), and the Program of Introducing Talents of Discipline to Universities (B06006) for financial support.

**Keywords:** Artificial photosynthesis • CO<sub>2</sub> reduction • Liquid fuels • CH<sub>3</sub>OH production • Cu/Cu<sub>2</sub>O interface

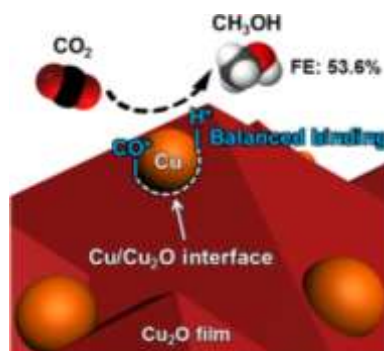
- [1] J. L. White, M. F. Baruch, J. E. Pander Iii, Y. Hu, I. C. Fortmeyer, J. E. Park, T. Zhang, K. Liao, J. Gu, Y. Yan, T. W. Shaw, E. Abelev, A. B. Bocarsly, *Chem. Rev.* **2015**, *115*, 12888-12935.
- [2] a) X. Chang, T. Wang, J. Gong, *Energy Environ. Sci.* **2016**, *9*, 2177-2196; b) S. N. Habisreutinger, L. Schmidt-Mende, J. K. Stolarczyk, *Angew. Chem. Int. Ed.* **2013**, *52*, 7372-7408; *Angew. Chem.* **2013**, *125*, 7516-7557.
- [3] a) E. E. Barton, D. M. Rampulla, A. B. Bocarsly, *J. Am. Chem. Soc.* **2008**, *130*, 6342-6344; b) M. Behrens, F. Studt, I. Kasatkin, S. Kuhl, M. Havecker, F. Abild-Pedersen, S. Zander, F. Girgsdies, P. Kurr, B. L. Kniep, M. Tovar, R. W. Fischer, J. K. Nørskov, R. Schlögl, *Science* **2012**, *336*, 893-897.

- [4] G. Ghadimkhani, N. R. de Tacconi, W. Chanmanee, C. Janaky, K. Rajeshwar, *Chem. Commun.* **2013**, *49*, 1297-1299.
- [5] W. Wei, Z. Yang, W. Song, F. Hu, B. Luan, P. Li, H. Yin, *J. Colloid. Interf. Sci.* **2017**, *496*, 327-333.
- [6] a) M. Schreier, F. Héroguel, L. Steier, S. Ahmad, J. S. Luterbacher, M. T. Mayer, J. Luo, M. Grätzel, *Nat. Energy* **2017**, *2*, 17087; b) A. Marimuthu, J. Zhang, S. Linic, *Science* **2013**, *339*, 1590-1593; c) J. Graciani, K. Mudiyansele, F. Xu, A. E. Baber, J. Evans, S. D. Senanayake, D. J. Stacchiola, P. Liu, J. Hrbek, J. F. Sanz, J. A. Rodriguez, *Science* **2014**, *345*, 546-550.
- [7] X. Chang, T. Wang, P. Zhang, Y. Wei, J. Zhao, J. Gong, *Angew. Chem. Int. Ed.* **2016**, *55*, 8840-8845; *Angew. Chem.* **2016**, *128*, 8986-8991.
- [8] a) Q. Fu, W. X. Li, Y. Yao, H. Liu, H. Y. Su, D. Ma, X. K. Gu, L. Chen, Z. Wang, H. Zhang, B. Wang, X. Bao, *Science* **2010**, *328*, 1141-1144; b) Z. W. Ulissi, M. T. Tang, J. Xiao, X. Liu, D. A. Torelli, M. Karamad, K. Cummins, C. Hahn, N. S. Lewis, T. F. Jaramillo, K. Chan, J. K. Nørskov, *ACS Catal.* **2017**, *7*, 6600-6608; c) T. Cheng, H. Xiao, W. A. Goddard, III, *J. Phys. Chem. Lett.* **2015**, *6*, 4767-4773; d) X. Nie, W. Luo, M. J. Janik, A. Asthagiri, *J. Catal.* **2014**, *312*, 108-122.
- [9] a) J. Albo, A. Sáez, J. Solla-Gullón, V. Montiel, A. Irabien, *Appl. Catal. B* **2015**, *176-177*, 709-717; b) M. Le, M. Ren, Z. Zhang, P. T. Sprunger, R. L. Kurtz, J. C. Flake, *J. Electrochem. Soc.* **2011**, *158*, E45.
- [10] a) S. Kattel, P. Liu, J. G. Chen, *J. Am. Chem. Soc.* **2017**, *139*, 9739-9754; b) X. Zhou, R. Liu, K. Sun, D. Friedrich, M. T. McDowell, F. Yang, S. T. Omelchenko, F. H. Saadi, A. C. Nielander, S. Yalamanchili, K. M. Papadantonakis, B. S. Brunshwig, N. S. Lewis, *Energy Environ. Sci.* **2015**, *8*, 2644-2649.
- [11] T. Wang, Y. Wei, X. Chang, C. Li, A. Li, S. Liu, J. Zhang, J. Gong, *Appl. Catal. B* **2018**, *226*, 31-37.
- [12] M. M. Hawkeye, M. J. Brett, *J. Vac. Sci. Technol. A* **2007**, *25*, 1317.
- [13] P. Yang, Z. J. Zhao, X. Chang, S. Zha, G. Zhang, R. Mu, J. Gong, *Angew. Chem. Int. Ed.* **2018**, DOI:10.1002/anie.201801463.
- [14] R. Reske, H. Mistry, F. Behafarid, B. Roldan Cuenya, P. Strasser, *J. Am. Chem. Soc.* **2014**, *136*, 6978-6986.
- [15] N. T. Hahn, H. Ye, D. W. Flaherty, A. J. Bard, C. B. Mullins, *ACS Nano* **2010**, *4*, 1977-1986.
- [16] J. Kunze, V. Maurice, L. H. Klein, H.-H. Strehblow, P. Marcus, *J. Phys. Chem. B* **2001**, *105*, 4263-4269.
- [17] S. Lee, D. Kim, J. Lee, *Angew. Chem. Int. Ed.* **2015**, *54*, 14701-14705; *Angew. Chem.* **2015**, *127*, 14914-14918.
- [18] D. Scarano, S. Bordiga, C. Lamberti, G. Spoto, G. Ricchiardi, A. Zecchina, C. Otero Areán, *Surf. Sci.* **1998**, *411*, 272-285.
- [19] B. Eren, C. Heine, H. Bluhm, G. A. Somorjai, M. Salmeron, *J. Am. Chem. Soc.* **2015**, *137*, 11186-11190.
- [20] Z. Zheng, B. Huang, Z. Wang, M. Guo, X. Qin, X. Zhang, P. Wang, Y. Dai, *J. Phys. Chem. C* **2009**, *113*, 14448-14453.
- [21] A. A. Peterson, F. Abild-Pedersen, F. Studt, J. Rossmeisl, J. K. Nørskov, *Energy Environ. Sci.* **2010**, *3*, 1311-1315.
- [22] L. Zhang, Z. J. Zhao, J. Gong, *Angew. Chem. Int. Ed.* **2017**, *56*, 11326-11353; *Angew. Chem.* **2017**, *129*, 11482-11511.

## Table of Contents

## COMMUNICATION

This communication describes how the Cu/Cu<sub>2</sub>O interface balances the binding strength of H<sup>+</sup> and CO\* intermediates for photoelectrochemical reduction of CO<sub>2</sub>, leading to a CH<sub>3</sub>OH Faradaic efficiency (FE) of 53.6% in aqueous conditions.



Xiaoxia Chang\*, Tuo Wang\*, Zhi-Jian Zhao, Piaoping Yang, Jeffrey Greeley, Rentao Mu, Gong Zhang, Zhongmiao Gong, Zhibin Luo, Jun Chen, Yi Cui, Geoffrey A. Ozin, and Jinlong Gong\*

Page No. – Page No.

Tuning Cu/Cu<sub>2</sub>O Interfaces for Reduction of Carbon Dioxide to Methanol in Aqueous Solutions